

The “Very-Near-Field” Region of Equiphase Radiating Apertures

S. Laybros^{1,2}, P. F. Combes¹, and H. J. Mametsa²

¹UPS-AD2M-IGEEP

118 route de Narbonne, 31062 Toulouse cedex, France
Tel: +33 6 88 78 06 33; E-mail: sarah_laybros@hotmail.com; pcombes@cict.fr

²ONERA-DEMR

BP 4025, 2 avenue E. Belin, 31055 Toulouse cedex, France
Tel: +33 5 62 25 27 07; E-mail: mametsa@onera.fr

Abstract

The purpose of this article is to investigate the so-called “near-field reactive” or “very-near-field” region of radiating apertures with different shapes and aperture illuminations. In this unusual and rather unknown region, we underline the specific behavior of the radiated fields, the wave impedance, and the power density. Thanks to these properties, we succeed in determining, in the first part, the outer boundary of the “very-near-field” region of a circular aperture with a uniform illumination law. Then, we review the influence of the illumination law and of the aperture shape on the extent of this region, through the cases of parabolic or cosine laws, and the case of square-shaped aperture. This study can find various applications in the wireless communications and radar antenna domains and, more recently, in electromagnetic compatibility problems.

Keywords: Antennas; apertures; aperture antennas; near field; electromagnetic fields

1. Introduction

This paper, devoted to equiphase radiating apertures, follows a previous article [1] concerning the radiation regions of short $\lambda/2$ and λ dipoles. These dipoles and apertures cover two important classes of antennas. Both articles have been written with the same aim: first, to accurately define the boundary of the so-called [2] “near-field reactive” or “very-near-field” region, and second, to analyze the electromagnetic characteristics (fields, wave impedance, power density) of the waves in this region.

According to IEEE standard definitions [2], an equiphase aperture for which D is the dimension in the E or H plane presents three different radiation regions. The first is the “far-field” region (or Fraunhofer region), at distances greater than $2D^2/\lambda$, where the angular field distribution is independent of the distance from the antenna and the radiated wave is spherical. The second is the “near-field radiating” region (or Fresnel region), at distances less than $2D^2/\lambda$, wherein the angular field distribution is dependent upon the distance from the antenna. In this region, the radiated wave, which is first a plane wave, is progressively transformed into a spherical wave. The third is the “near-field reactive” region, located between 0 and $\lambda/2\pi$ from the antenna, wherein the reactive field predominates.

Moreover, some authors [3, 4] distinguish, inside the Fresnel region, the Rayleigh region, at distances less than $D^2/2\lambda$. In this region, the radiation is concentrated inside a tubular beam, and the

radiated wave is quasi-planar. This region may be relatively large, since if $D = 100\lambda$, $D^2/2\lambda$ increases to 5000λ (for instance, $D^2/2\lambda = 150\text{ m}$ for $D = 3\text{ m}$ and $\lambda = 3\text{ cm}$).

It is worthwhile to make the definition of the outer boundary of the “near-field reactive” region more precise, because the $\lambda/2\pi$ criterion of the IEEE standard definition seems to us to be questionable. Besides, some authors find it underestimated. Hansen [5, p. 33] wrote: “It has been *assumed* that from large aperture antennas, the reactive fields are very small when they are 1λ away so that the boundary between the reactive and radiating near field regions has been *conservatively* taken as $r = \lambda$.” Yaghjian [6, p. 33] pointed out that “the reactive near-field region is commonly taken to extend about $\lambda/2\pi$ from the surface of the antenna, although experience with near-field measurements indicates that a distance of a wavelength (λ) or so would form a more reasonable outer boundary of the reactive near-field.” As far as he is concerned, Balanis [7, p. 117] determined this boundary to be $0.62\sqrt{D^3/\lambda}$. His demonstration was based on an asymptotic development over the distance, r , between the antenna and the calculation point. The corresponding approximations lead to an error in the phase term, $\exp(-jkr)$, which is involved in field computation integrals. However, there is no direct relationship between this error and the errors that are induced by it in the characteristics of the radiated waves (fields, wave impedance, power density).

In this paper, we explain (Section 2) the theoretical basis of our work and the criteria we have chosen for the determination of the outer boundary of the “near-field reactive” or “very-near-field” region. The reference case of an equiphase circular aperture with a uniform illumination law is first studied in Section 3.1. For this aperture, we define the “very-near-field” region as an interference region, inside which the radiated wave presents the following characteristics: the electric and magnetic fields are out of phase; the wave impedance is different from 120π (i.e., the free-space impedance); and the power density has a complex formulation, with a real part and an imaginary part. This region is extended up to one-quarter of the Rayleigh distance: up to $D^2/8\lambda$. Then, the influences of the illumination law and of the aperture shape on the boundary of this region are pointed out in Sections 3.3 and 3.4. Finally, the main characteristics of the wave, such as the wave impedance and the complex radiated power, are emphasized in the “very-near-field” region of a circular aperture (Section 4) and of a square aperture (Section 5). These features are studied not only along the longitudinal axis, but also on the transverse planes. In conclusion, this new definition of the “very-near-field” region is integrated into a simple classification of the radiation regions we propose.

Our work is not only of *academic interest*, because it reconsiders the range of the “very-near-field” region of aperture antennas, but it is also of *practical interest*, because the problem of direct or indirect radiation of antennas in their vicinity is of growing interest. These investigations thus can find various applications in the wireless communication systems and radar antenna domains. More recently, inter-system EM interference on high-level integration platforms (ship types), and the EM environment produced by various radio-frequency equipment (airport types), which may affect significantly functional system performance require the prediction and the evaluation of the surrounding EM fields.

2. Theoretical Basis

2.1 Expressions of the Radiated Fields

We aim to compute the electric and magnetic fields radiated by a plane surface carrying electric and magnetic surface currents

$$\begin{aligned}\vec{I}_S &= \hat{n} \times \vec{H}, \\ \vec{I}_S^m &= -\hat{n} \times \vec{E}.\end{aligned}\quad (1)$$

These are defined at a point, Q, of this surface, where \hat{n} is the unit normal to the surface. According to Huygens' principle, these currents radiate some elementary spherical waves. The electric and magnetic vector potentials induced at a point P are

$$\vec{A}(P) = \frac{\mu}{4\pi} \int_S \vec{I}_S(Q) \frac{\exp(-jkr)}{r} dS, \quad (2)$$

$$\vec{A}_m(P) = \frac{\varepsilon}{4\pi} \int_S \vec{I}_S^m(Q) \frac{\exp(-jkr)}{r} dS. \quad (3)$$

We denote $r = QP$ and $\hat{r} = \vec{r}/r$. The time dependence is through the factor $\exp(j\omega t)$.

In accordance with Maxwell's equations [8], the electric harmonic field radiated at the point P can be expressed as follows:

$$E(P) = -j\omega \vec{A} - \frac{j}{\omega\varepsilon\mu} \vec{\nabla}(\vec{\nabla} \cdot \vec{A}) - \frac{1}{\varepsilon} \vec{\nabla} \times \vec{A}_m, \quad (4)$$

or, in a shorter form,

$$\vec{E}(P) = -\frac{j}{\omega\varepsilon\mu} \vec{\nabla} \times \vec{\nabla} \times \vec{A} - \frac{1}{\varepsilon} \vec{\nabla} \times \vec{A}_m. \quad (5)$$

Notice that the magnetic-field expression can be obtained according to the duality principle by substituting \vec{A}_m for \vec{A} , $-\vec{A}$ for \vec{A}_m , and ε for μ or μ for ε in Equations (4) and (5).

Using the relations of Equations (2)-(4) and $\psi = \exp(-jkr)/r$, we obtain the expression

$$\begin{aligned}\vec{E}(P) &= -\frac{j\omega\mu}{4\pi} \int_S \vec{I}_S(Q) \psi dS - \frac{j}{4\pi\varepsilon\omega} \int_S \vec{\nabla}[\vec{\nabla} \cdot \vec{I}_S(Q) \psi] dS \\ &\quad - \frac{1}{4\pi} \int_S \vec{\nabla} \times \vec{I}_S^m(Q) \psi dS,\end{aligned}\quad (6)$$

which we can also express as

$$\begin{aligned}\vec{E}(P) &= -\frac{j\omega\mu}{4\pi} \int_S \vec{I}_S(Q) \psi dS - \frac{j}{4\pi\varepsilon\omega} \int_S [\vec{I}_S(Q) \cdot \vec{\nabla}] \vec{\nabla} \psi dS \\ &\quad + \frac{1}{4\pi} \int_S \vec{I}_S^m(Q) \times \vec{\nabla} \psi dS.\end{aligned}\quad (7)$$

This last expression, first established by Kottler in 1923 [9], was demonstrated in 1939 by Stratton and Chu [10], thanks to the Green vectorial theorem.

To calculate the second and the third terms in Equation (6), it is important to point out that \vec{I}_S and \vec{I}_S^m only depend on the point Q, and that the operator $\vec{\nabla}$ acts on the point P (where the unit vector in the direction \vec{PQ} must be denoted $-\hat{r}$). Under these conditions,

$$\vec{\nabla} \cdot \vec{I}_S \psi = \psi \vec{\nabla} \cdot \vec{I}_S + \vec{I}_S \cdot \vec{\nabla} \psi = \vec{I}_S \cdot \vec{\nabla} \psi = \left(jk + \frac{1}{r}\right) \psi (\vec{I}_S \cdot \hat{r})$$

$$\begin{aligned}\vec{\nabla}(\vec{\nabla} \cdot \vec{I}_S \psi) &= \vec{\nabla}(\vec{I}_S \cdot \vec{\nabla} \psi) = k^2 \left(-1 + \frac{3j}{kr} + \frac{3}{k^2 r^2}\right) \psi (\vec{I}_S \cdot \hat{r}) \hat{r} \\ &\quad - k^2 \left(\frac{j}{kr} + \frac{1}{k^2 r^2}\right) \psi \vec{I}_S\end{aligned}\quad (8)$$

$$\vec{\nabla} \times \vec{I}_S^m \psi = \psi \vec{\nabla} \times \vec{I}_S^m - \vec{I}_S^m \times \vec{\nabla} \psi = -\vec{I}_S^m \times \vec{\nabla} \psi = \left(jk + \frac{1}{r}\right) \psi (\vec{I}_S^m \times \hat{r}).$$

These expressions are similar to those given in the classical references such as, for instance, Silver [11]. Considering that

$$\omega\mu = kZ \quad \text{and} \quad \omega\varepsilon = \frac{k}{Z}, \quad (9)$$

where $Z = \sqrt{\mu/\varepsilon}$ is the wave impedance in the media being studied media and $k = \omega\sqrt{\varepsilon\mu}$, the expression of Equation (2.5) becomes

$$\begin{aligned} \vec{E}(P) = & -j \frac{k^2}{4\pi} \int_S \left[Z \left(1 - \frac{j}{kr} - \frac{1}{k^2 r^2} \right) \left[\hat{n} \times \vec{H}(Q) \right] \right. \\ & + Z \left(-1 + \frac{3j}{kr} + \frac{3}{k^2 r^2} \right) \left\{ \hat{r} \cdot \left[\hat{n} \times \vec{H}(Q) \right] \right\} \hat{r} + \left(1 - \frac{j}{kr} \right) \hat{r} \times \left[\hat{n} \times \vec{E}(Q) \right] \Bigg] \\ & \frac{\exp(-jkr)}{kr} dS. \end{aligned} \quad (10)$$

2.2 Definition of the “Very-Near-Field” Region

In air or vacuum ($Z_0 = 120\pi$), at a distance r such as $kr = 1$, i.e., $r = \lambda/2\pi$, Equation (10) becomes

$$\begin{aligned} \vec{E}(P) = & -j \frac{k^2}{4\pi} \int_S \left\{ -jZ_0 (\hat{n} \times \vec{H}) + Z_0 (2 + 3j) \left[\hat{r} \cdot (\hat{n} \times \vec{H}) \right] \hat{r} \right. \\ & \left. + (1 - j) \hat{r} \times (\hat{n} \times \vec{E}) \right\} \exp(-jkr) dS. \end{aligned} \quad (11)$$

The dual expression for the magnetic field is

$$\begin{aligned} \vec{H}(P) = & -j \frac{k^2}{4\pi} \int_S \left\{ \frac{j}{Z_0} (\hat{n} \times \vec{E}) - \frac{1}{Z_0} (2 + 3j) \left[\hat{r} \cdot (\hat{n} \times \vec{E}) \right] \hat{r} \right. \\ & \left. + (1 - j) \hat{r} \times (\hat{n} \times \vec{H}) \right\} \exp(-jkr) dS. \end{aligned} \quad (12)$$

Consequently, the Poynting vector, $\vec{p} = \frac{1}{2} \vec{E} \times \vec{H}^*$, is a complex vector. A direct computation of this has shown us that for various apertures the real and the imaginary parts of \vec{p} are nearly equal. So, we can say that at the distance $r = \lambda/2\pi$ there is as much reactive as active power density. Thus, this distance cannot represent the end of the “near-field-reactive” region, as mentioned in the standard definitions of the IEEE [2]. According to us, it seems more convenient to investigate the distance at which the ratio between the reactive and the active power density becomes lower than -30 dB, for example. Beyond this distance, we could consider that the reactive power density is negligible. Moreover, for the same reason as why \vec{p} is complex, the wave impedance, which is the ratio between E and H , is also complex. This feature could also characterize the “near-field-reactive” region.

So, we think that the distance beyond which

- the reactive power density is negligible
- the wave impedance is equal to 120π

would really show the limit of the “near-field-reactive” region.

As we will see in Section 3, the fact that these two electromagnetic characteristics, \vec{p} and Z , are complex is linked to an interference phenomenon of the fields near the aperture. In the reference case of a circular aperture with uniform illumination, such interference is noteworthy, and may be interpreted thanks to the Huygens-Fresnel principle (Section 3.2). This will allow us to conclude that the “near-field-reactive” region is located between 0 and $D^2/8\lambda$, i.e., one-quarter of the Rayleigh distance. We suggest calling this region the “very-near-field” region, since it represents a part of the “near-field or Rayleigh” region (extended up to $D^2/2\lambda$, for a surface of dimension D in the E or H plane).

2.3 Computational Method

To evaluate this field in an efficient computational time, we use the method validated in [12]. The studied surface is divided into square elementary surfaces, S_n , of which the dimension, D_n , is narrow enough so as to consider that any observation point in the “near-field” or in the “very-near-field” region of the surface is in the “far-field” region of each elementary region (see Figure 1). In this case, the integral in Equation (10) can be simplified. Indeed, if the observation point is in the far-field region of the elementary surfaces, we can apply the following classic approximations to the amplitude terms (see Figure 2):

- The observation distance, $r = QP$, is approximated by the distance $O_n P$ (O_n the center of the surface);
- The scattering direction, $\hat{r} = \overrightarrow{QP} / \|\overrightarrow{QP}\|$, is approximated by

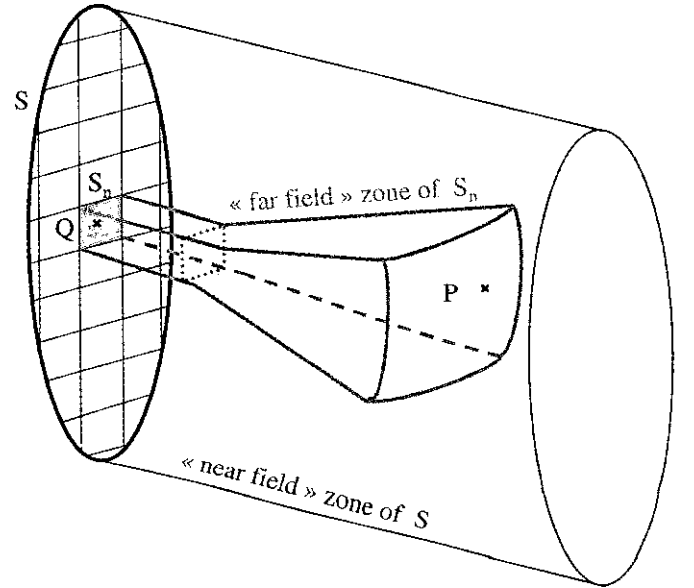


Figure 1. The subdivision of the radiating surface.

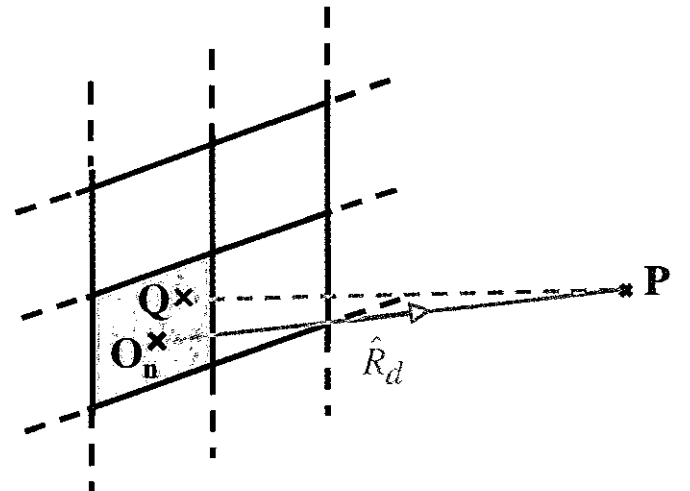


Figure 2. The geometric configuration for an elementary cell.

$$\hat{R}_d = \overline{O_n P} / \|\overline{O_n P}\|. \quad (13)$$

Under these conditions, both of these do not depend on the integration point. Notice that no approximation is made regarding the phase terms.

Moreover, if these elementary surfaces are small enough so that it can be considered that the field magnitude is constant inside their outline, the integral can even be simplified. The field magnitude on each elementary surface can be approximated by the magnitude of the field at the center of each surface:

$$\vec{E}(\mathcal{Q}) = \vec{E}_0(O_n) \exp(j\alpha_i) \quad (14a)$$

and

$$\vec{H}(\mathcal{Q}) = \vec{H}_0(O_n) \exp(j\alpha_i). \quad (14b)$$

α_i is the field phase, constant all along the surface (here, we are dealing with the case of the equiphase surface). So, $\vec{E}_0(O_n)$ and $\vec{H}_0(O_n)$ do not depend on the integration point.

Using Equations (13)-(14) in Equation (10), the expression of the electric field scattered by an elementary surface is

$$\vec{E}(P) = -j \frac{k^2}{4\pi} \mathcal{A} \frac{\exp(-jkO_n P)}{O_n P} \exp(j\alpha_i) \int_{S_n} \exp(jk\hat{R}_d \cdot \overline{O_n Q}) dS \quad (15)$$

with

$$\begin{aligned} \mathcal{A} = & Z \left(1 - \frac{j}{kO_n P} - \frac{1}{k^2 O_n P^2} \right) [\hat{n} \times \vec{H}_0(O_n)] \\ & + Z \left(-1 + \frac{3j}{kO_n P} + \frac{3}{k^2 (O_n P)^2} \right) \left\{ \hat{R}_d \cdot [\hat{n} \times \vec{H}_0(O_n)] \right\} \hat{R}_d \\ & + \left(1 - \frac{j}{kO_n P} \right) \hat{R}_d \times [\hat{n} \times \vec{E}_0(O_n)]. \end{aligned} \quad (16)$$

The integral term in this equation is now simplified. Furthermore, this surface integral can be reduced to a linear integral along the outline of the elementary surfaces thanks to the Stokes formula, which considerably moderates the computational time.

Finally, the total field is the vectorial and coherent sum of all the elementary surface contributions:

$$\vec{E}(P) = \sum_n \vec{E}_n(P). \quad (17)$$

Besides this, we have to divide the apertures into a sufficient number of domains to reconstruct the expected shape (circular or square). In order to draw upon an optimum number of domains, we use elements with different dimensions. The central elementary domains are adequate for considering the observation point to be in their far-field region, but as large as possible in order to restrict the number of computations. The elements close to the outline are smaller, to recreate the aperture shape (see Figure 3).

In this way, we can obtain an optimum way to compute the fields radiated by an aperture: this method allows a computation that is accurate and fast. To confirm these results, they were

successfully compared with the fields obtained from the exact integral computation of the expression (Equation 10), which requires a computation time about thirty times longer than our method.

We talk here about an aperture, but it is interesting to point out that this study can also concern a material surface, carrying a distribution of currents.

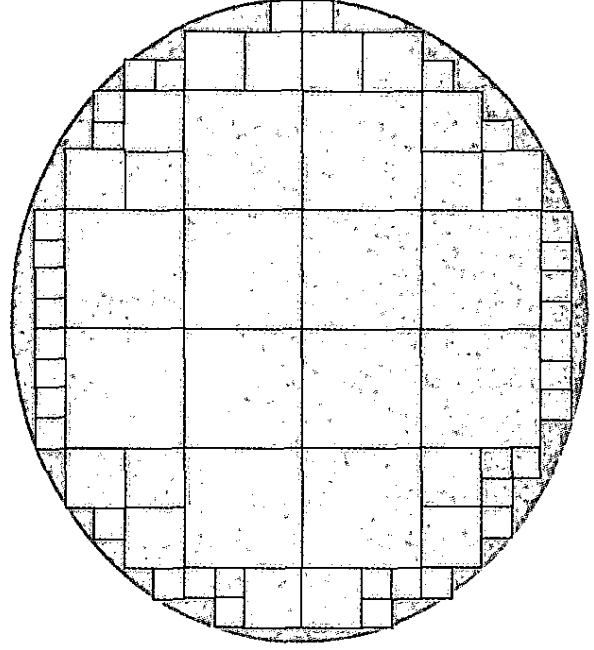


Figure 3a. The subdivision of the circular aperture.

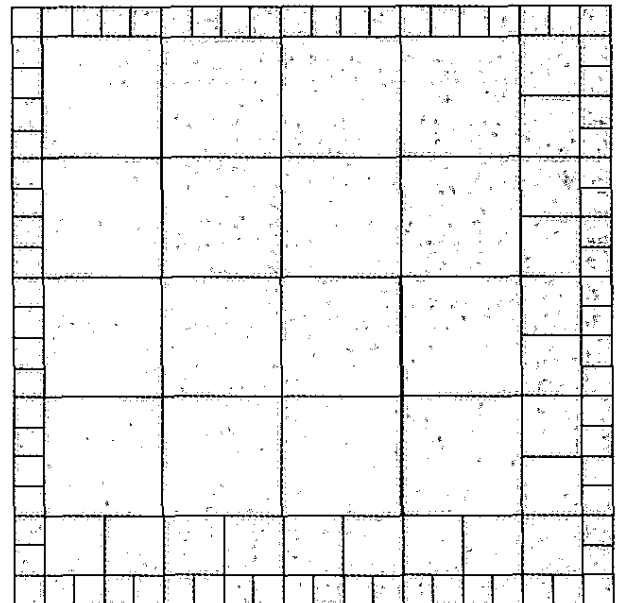


Figure 3b. The subdivision of the square aperture.

3. Emphasis on the “Very-Near-Field” Region

3.1 The Reference Case: A Circular Aperture with a Uniform Illumination

The variations of the E field radiated by an aperture along the central perpendicular axis are displayed in Figure 4. This is for a circular surface for which the diameter is equal to 10λ . We can clearly identify the three conventional radiation regions, mentioned in the introduction. Beyond $2D^2/\lambda = 200\lambda$, we can find the “far-field” region. The wave is spherical, and presents a decrease proportional to $1/r$. Up to $D^2/2\lambda = 50\lambda$, in the “near-field” or “Rayleigh” region, the wave is considered to be quasi-planar. Between these two regions, there is the intermediate region where the quasi-plane wave progressively becomes a spherical wave. If we now focus our attention on the behavior of the electric field nearer the aperture, we can observe some definite interference: this is the region we call the “very-near-field” region.

We aim to investigate this interference region. Figure 5 shows the field scattered from a circular surface of radius 5λ ($D=10\lambda$) in the “near field” region (from 0 up to $Rr = D^2/2\lambda = 50\lambda$, the Rayleigh distance). This field, observed along the central perpendicular axis, presents first and clearly some interference between 0 and $Rr/4 = 12.5\lambda$.

The cases of surfaces for which the radius is 10λ ($D=20\lambda$) and 25λ ($D=50\lambda$) are also displayed in Figures 6 and 7. According to these figures, we can notice that for an aperture of radius $n\lambda$ (n is an integer), we can see $n-1$ interference lobes surrounded with n minima, of which the last one is exactly located at $Rr/4$. For apertures for which the radius is 5λ , 10λ , 25λ , the distance $Rr/4$ is respectively 12.5λ , 50λ , and 312.5λ . Beyond this limit, the field magnitude increases, reaches its last maximum approximately at $Rr/2$, and begins to decrease. This is not a supplementary interference lobe, since it presents a $1/r^\alpha$ decrease ($0 < \alpha \leq 1$) and tends to zero at infinity. All these properties have been checked for other dimensions of the aperture.

So, inside the classic “near-field” region (or Rayleigh region), the “very-near-field” region, stretched as far as one-quarter of the Rayleigh distance, has to be emphasized: this is a region of interference, inside which the electric and magnetic fields present some important magnitude variations.

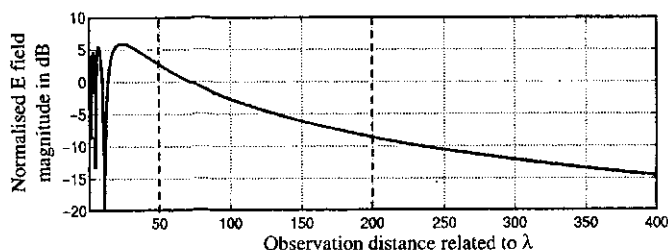


Figure 4. Variations of the E -field magnitude along the central perpendicular axis.

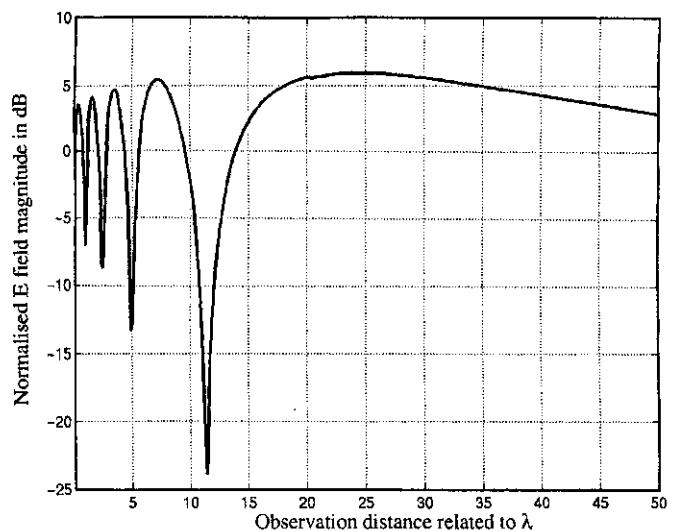


Figure 5. The interference lobes in the “very-near-field” region of a 5λ radius circular aperture.

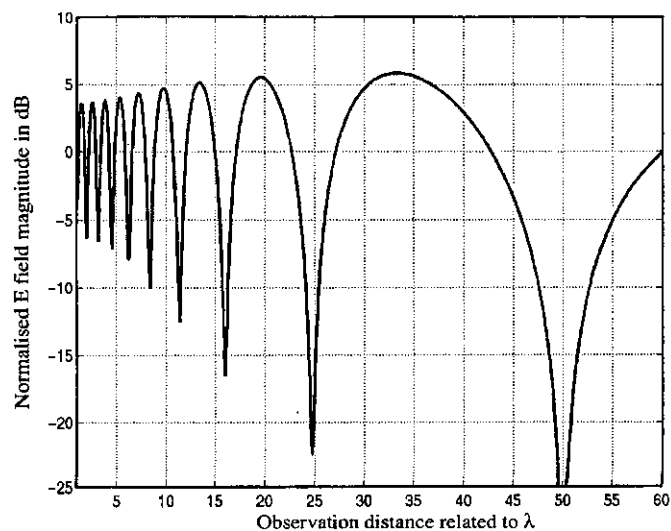


Figure 6. The interference lobes in the “very-near-field” region of a 10λ radius circular aperture.

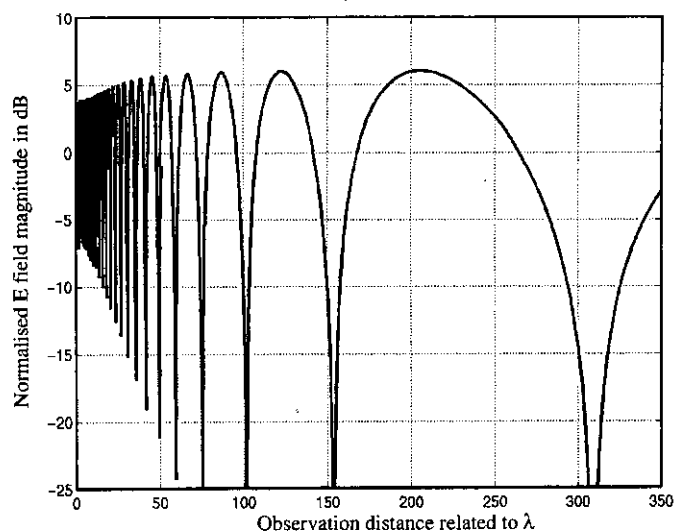


Figure 7. The interference lobes in the “very-near-field” region of a 25λ radius circular aperture.

3.2 Interpretation of the Interference Phenomena

These phenomena can be interpreted by means of the Huygens-Fresnel principle. Depending on the observation distance along the central perpendicular axis of the aperture, we could define the *Fresnel zones* fitting in with this aperture. These zones will allow representation of the radiation of a $D = N\lambda$ diameter equiphase aperture.

3.2.1 Definition of the Rayleigh Distance

Let us consider an equiphase circular aperture for which the diameter is $D = BB' = 2OB$, and a point P on the Oz axis, such as $OP = R$ (Figure 8). Rayleigh investigated the distance $R = Rr$, where the path difference $BP - OP = \lambda/4$; this corresponds to a phase difference of $\pi/2$ between the fields radiated at the point P by the Huygens sources located at O and B. A simple calculation leads to the Rayleigh distance, equal to $D^2/2\lambda$, using the approximation

$$\sqrt{1 + \frac{D^2}{4R^2}} \approx 1 + \frac{D^2}{8R^2}. \quad (18)$$

This approximation seems reasonable (with an error lower than 1%), as soon as $R > 1.6D = 1.6N\lambda$.

3.2.2 Justification of the Minimum Observed at $Rr/4$

Let us consider a point P on the Oz axis so that the path difference is $BP - OP = \lambda$. We can easily demonstrate that $OP = Rr/4$, at least if the condition $R > 1.6\lambda$ is fulfilled. The relative phase shift between the fields radiated at P by the two Huygens sources located at O and B (B') is

$$\Delta\phi = \frac{2\pi}{\lambda} \lambda = 2\pi. \quad (19)$$

We can also define two symmetric points on the aperture, B_1 and B_1' in Figure 9, such that $B_1P - OP = \lambda/2$ ($= B_1'P - OP$). So,

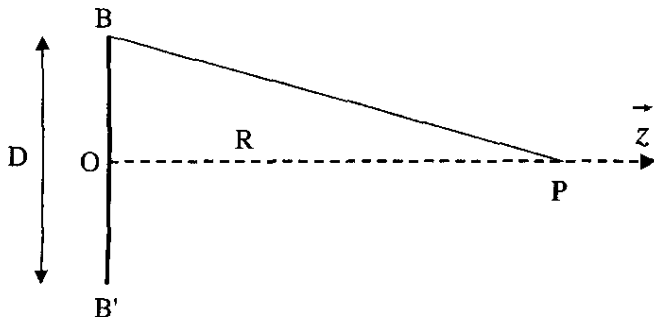


Figure 8. The configuration for the Rayleigh distance.

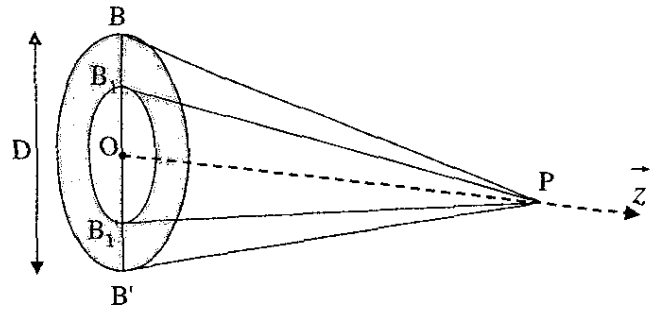


Figure 9. The two first Fresnel zones.

the relative phase shift between the fields radiated by the Huygens sources located at O and B_1 (or B_1'), is equal to π .

- The part of the aperture between B_1 and B_1' represents the first *Fresnel zone* (in the clear region in Figure 9). The fields radiated by the sources of this zone at the point P present an *average phase* equal to $\phi_1 = \phi_0 + \frac{\pi}{2}$; ϕ_0 is the reference phase of the field radiated by the source situated at O. Thus, the field radiated by this first *Fresnel zone* is

$$E_1(P) = E_1 \exp[-j(\phi_0 + \pi/2)]. \quad (20)$$

- The part of the aperture illustrated by the exterior corona (in the dark region in Figure 9) represents the second *Fresnel zone*. The sources inside this zone radiate at P a field with an *average phase* equal to $\phi_2 = \phi_0 + \frac{3\pi}{2}$. This field, due to the second *Fresnel zone*, is

$$E_2(P) = E_2 \exp[-j(\phi_0 + 3\pi/2)]. \quad (21)$$

As a result, these two zones radiate two fields with opposite phases at the point P: the resultant field is a minimum. It is not nil, because $E_2 < E_1$, since the magnitude of the fields due to the *Fresnel zones* depends on an obliquity factor equal to $\frac{1 + \cos\theta}{2}$ (θ is the angle between the direction B_1P or BP and the Oz axis).

3.2.3 Justification of the Magnitude Maxima at $Rr/2$ and $Rr/8$

The maximum located at $Rr/2$ ($Rr/8$) corresponds to a point P such that $BP - OP = \lambda/2$ ($3\lambda/2$). Notice that the condition $R > 1.6\lambda$ has still to be fulfilled. If this is not true – in particular, concerning the second case – the point P would be a little bit further than $Rr/8$.

- At $Rr/2$, the phase shift between the fields radiated by the sources situated at O and B is $\Delta\phi = \pi$. Only the first *Fresnel zone* can be defined inside the aperture, for which the *average phase* is equal to $\phi_0 + \frac{\pi}{2}$. In comparison to the previous case, the radiation of the second *Fresnel zone* with an opposite phase is lacking. That is the reason why we meet a maximum at $Rr/2$.

• At $Rr/8$, the relative phase shift between the fields radiated by the sources situated at O and B is $\Delta\phi = 3\pi$. Consequently, we can fit three *Fresnel zones* into the aperture: these three zones are bounded by the points corresponding to the phase shifts equal to $\Delta\phi = \pi, 2\pi, 3\pi$. The radiated fields present *average phases* that are $\phi_0 + \frac{\pi}{2}$, $\phi_0 + \frac{3\pi}{2}$, $\phi_0 + \frac{5\pi}{2}$. The two first *Fresnel zones* fields cancel each other out. The field due to the third zone induces the maximum present at $Rr/8$:

$$\underline{E}_3(P) = E_3 \exp[-j(\phi_0 + 5\pi/2)]. \quad (22)$$

This last field amplitude is lower than the one seen at $Rr/2$ because of the obliquity factor. It is smaller in this case ($Rr/8$), where the observation point is closer to the aperture.

3.2.4 Interpretation of the Other Maxima and Minima

For each point P corresponding to an even number of *Fresnel zones*, the field radiated by the aperture is a minimum because the fields radiated by two adjacent zones are canceling each other out. On the contrary, for each point P corresponding to an odd number of *Fresnel zones*, the field is a maximum. In this case, there is always one zone for which the radiated field is not cancelled.

So, in the case of an aperture for which the diameter can be written $D = N\lambda$, we can define N different *Fresnel zones*, at most. The total number of maxima and minima situated up to $Rr/4$ is $N-1$:

- If N is even, there are $\frac{N}{2}$ minima and $\frac{N}{2}-1$ maxima, with a minimum on the aperture;
- If N is odd, there are $\frac{N-1}{2}$ minima and $\frac{N-1}{2}$ maxima, with a maximum on the aperture.

3.3 The Influence of Aperture Illumination

We now study the influence of the aperture-illumination law. This is why we determine the “very-near-field” region upper boundary for circular apertures with a nonuniform illumination. As for the uniform circular case, the “very-near-field” region boundary will be set at the distance where the field magnitude reaches its last minimum.

Four nonuniform equiphase laws are reviewed here: parabolic, squared parabolic, cosine, and squared cosine distributions. The expressions of these illumination laws, $\mathcal{A}(\rho)$, are specified in Table 1, where ρ represents the distance between a point Q and the center of the aperture. Figure 10 displays the variations of the E -field magnitude along the central axis in the case of a 10λ radius circular surface with the four different illumination laws. We can notice that the variations present less pronounced peaks than for the uniform case. Referring to Section 3.2 and due to these illuminations, the fields of each *Fresnel zone* do not present the

Table 1. The expressions for the four illuminations studied and their “very-near-field” region boundaries.

Illumination	Aperture Distribution	Boundary
Uniform	$\mathcal{A}(\rho) = 1$	$Rr/4 = D^2/8\lambda$
Parabolic	$\mathcal{A}(\rho) = 1 - \left(\frac{\rho}{D/2}\right)^2$	$0.82D^2/8\lambda$
Squared parabolic	$\mathcal{A}(\rho) = \left(1 - \left(\frac{\rho}{D/2}\right)^2\right)^2$	$0.70D^2/8\lambda$
Cosine	$\mathcal{A}(\rho) = \cos \frac{\pi\rho}{D}$	$0.81D^2/8\lambda$
Squared cosine	$\mathcal{A}(\rho) = \cos^2 \frac{\pi\rho}{D}$	$0.69D^2/8\lambda$

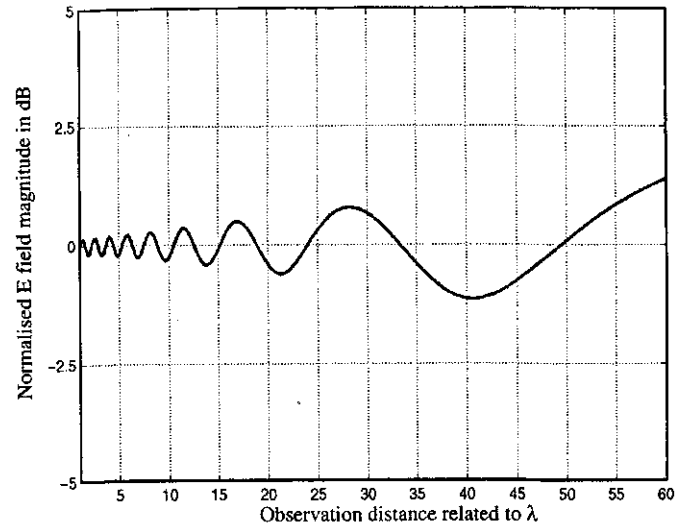


Figure 10a. The axial magnitude of the E field for an aperture of radius equal to 10λ ($Rr/4 = 50\lambda$), with parabolic illumination.

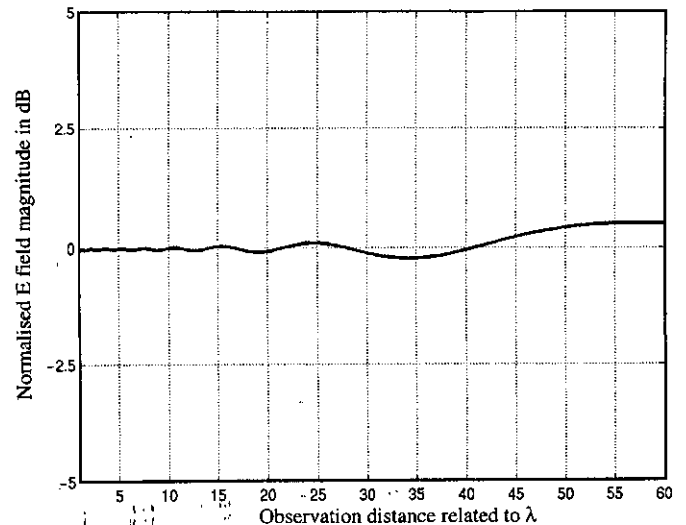


Figure 10b. The axial magnitude of the E field for an aperture of radius equal to 10λ ($Rr/4 = 50\lambda$), with squared parabolic illumination.

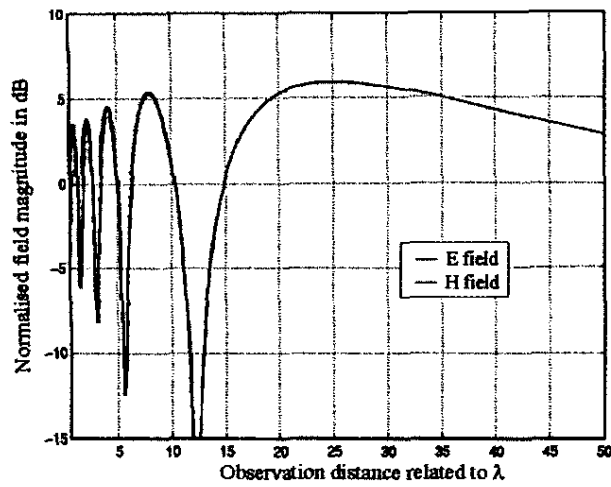


Figure 12. The E and H interference lobes in the “very-near-field” region of a 5λ radius aperture.

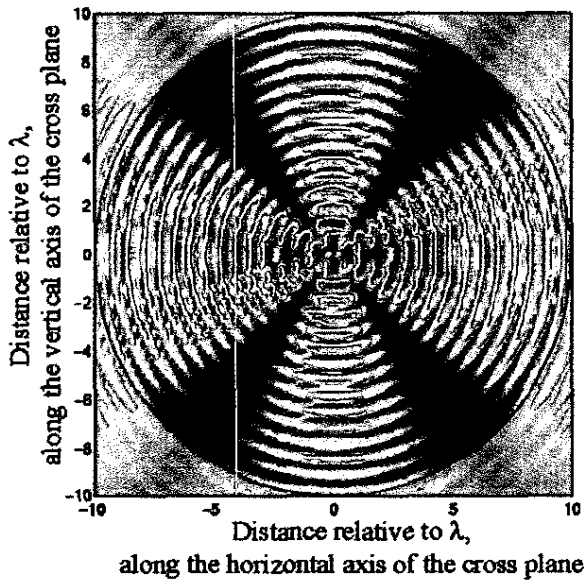


Figure 16a. The variations of the wave-impedance criterion $|Z - Z_0|/Z_0$ for a 10λ radius aperture ($Rr/4 = 50\lambda$) on the transverse plane at 15λ from the aperture.

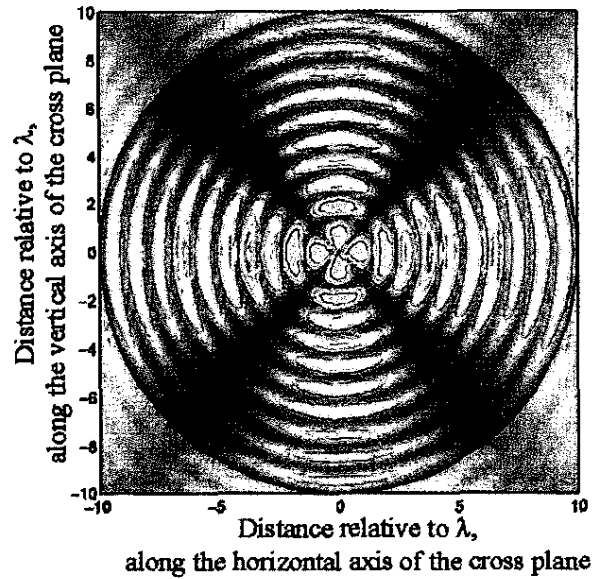


Figure 16b. The variations of the wave-impedance criterion $|Z - Z_0|/Z_0$ for a 10λ radius aperture ($Rr/4 = 50\lambda$) on the transverse plane at 30λ from the aperture.

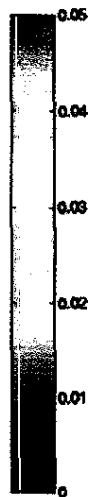
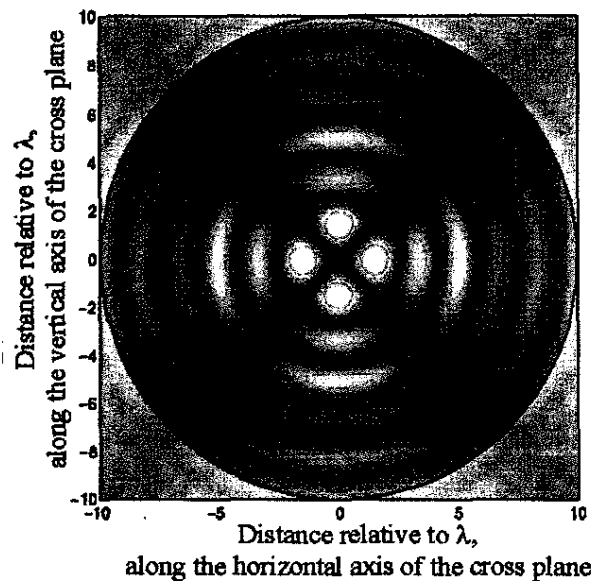


Figure 16c. The variations of the wave-impedance criterion $|Z - Z_0|/Z_0$ for a 10λ radius aperture ($Rr/4 = 50\lambda$) on the transverse plane at 60λ from the aperture.



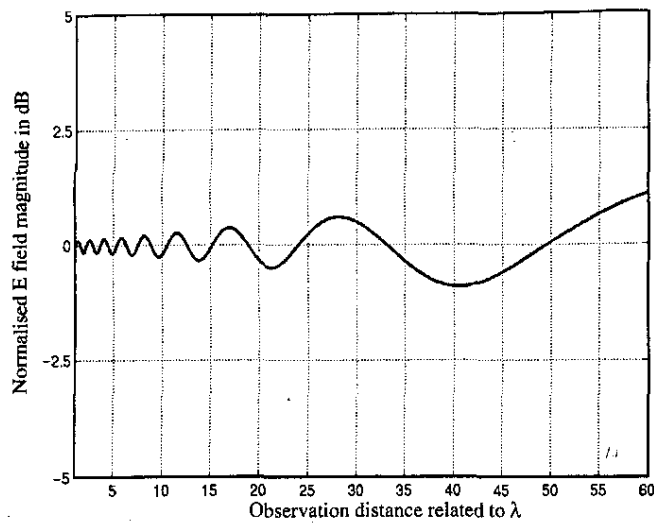


Figure 10c. The axial magnitude of the E field for an aperture of radius equal to 10λ ($Rr/4 = 50\lambda$), with cosine illumination.

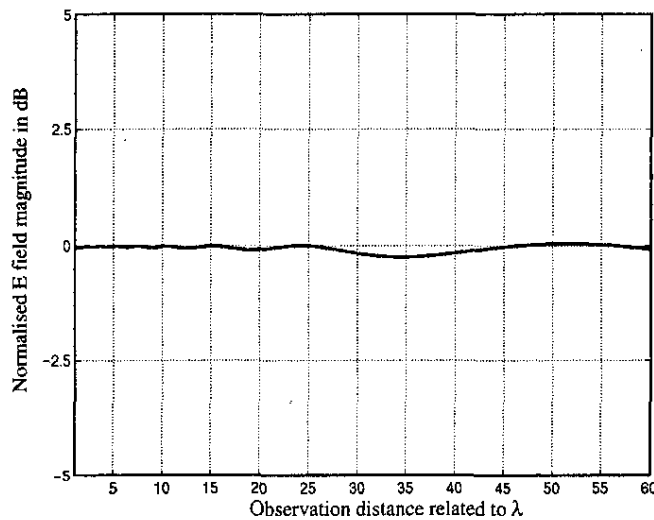


Figure 10d. The axial magnitude of the E field for an aperture of radius equal to 10λ ($Rr/4 = 50\lambda$), with squared cosine illumination.

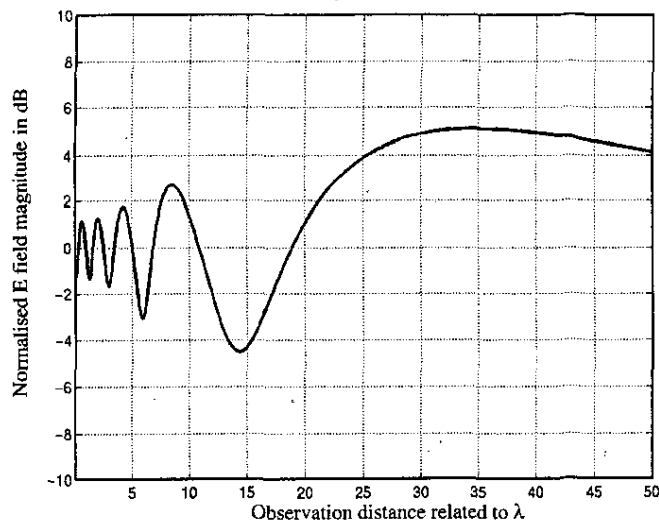


Figure 11a. The axial magnitude of the E field for a 10λ wide ($Rr/4 = 12.5\lambda$) square aperture.

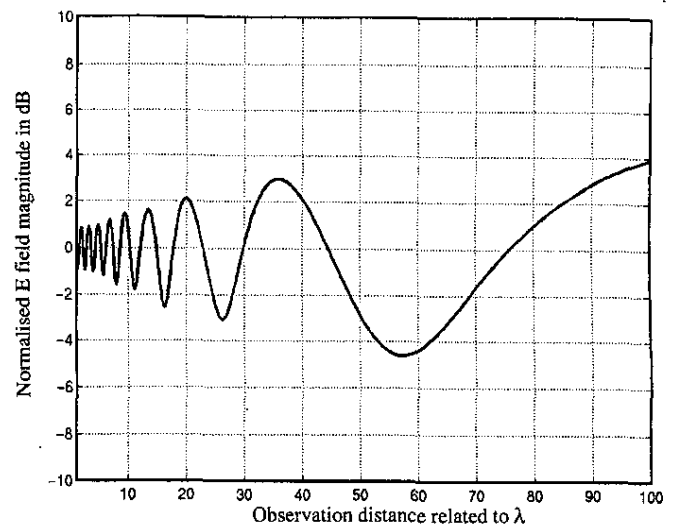


Figure 11b. The axial magnitude of the E field for a 20λ wide ($Rr/4 = 50\lambda$) square aperture.

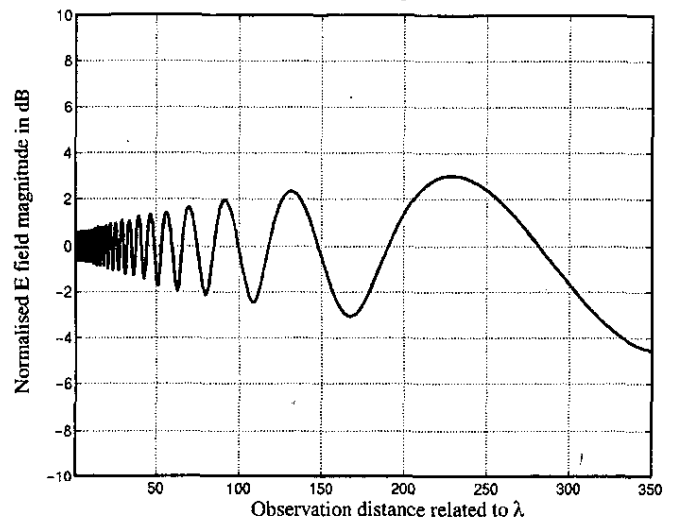


Figure 11c. The axial magnitude of the E field for a 50λ wide ($Rr/4 = 312.5\lambda$) square aperture.

same magnitude, which decreases and tends to zero on the edge of the aperture. So, even if the fields from the *Fresnel zones* have opposite phases, their magnitudes do not have the same weight. This explains why the interference phenomena are all the more damped as the illumination law is tapered.

Even so, it is still possible to determine the location of the last minimum. For the 10λ radius aperture presented here, we succeeded in concluding with a coefficient applied to $Rr/4$. Indeed, for the parabolic law, for example, the last minimum is located at $0.82 Rr/4$. We checked the validity of this coefficient for apertures of radii equal to 5λ , 10λ , 25λ , and 50λ . For all studied illumination laws, the coefficients are noted in Table 1. Notice that they are all lower than 1.

So, reasoning in the same way as for the uniform-illumination aperture, we determined the upper boundary of the “very-near-field” region of apertures with a nonuniform illumination. These boundaries are defined as a fraction of a quarter of the Rayleigh distance, Rr .

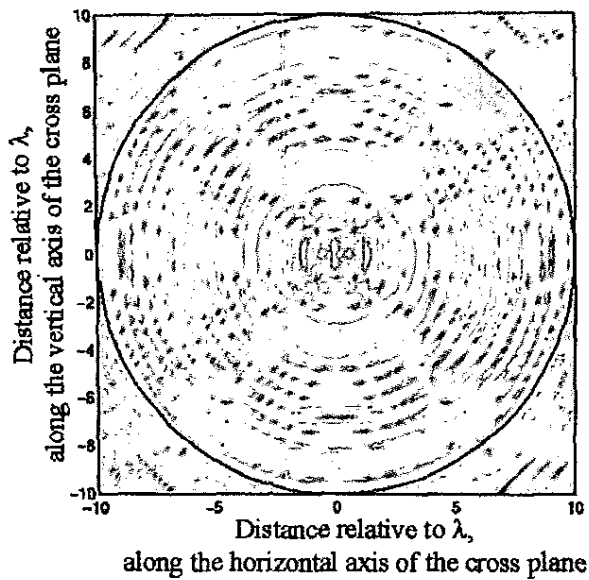


Figure 17a. The variations of the power-density criterion p_r/p_a for a 10λ radius aperture ($Rr/4 = 50\lambda$) on the transverse plane at 15λ from the aperture.

Figure 17b. The variations of the power-density criterion p_r/p_a for a 10λ radius aperture ($Rr/4 = 50\lambda$) on the transverse plane at 30λ from the aperture.

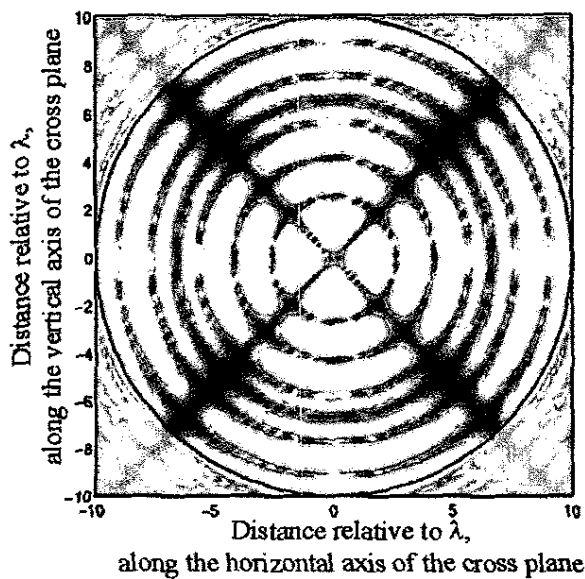
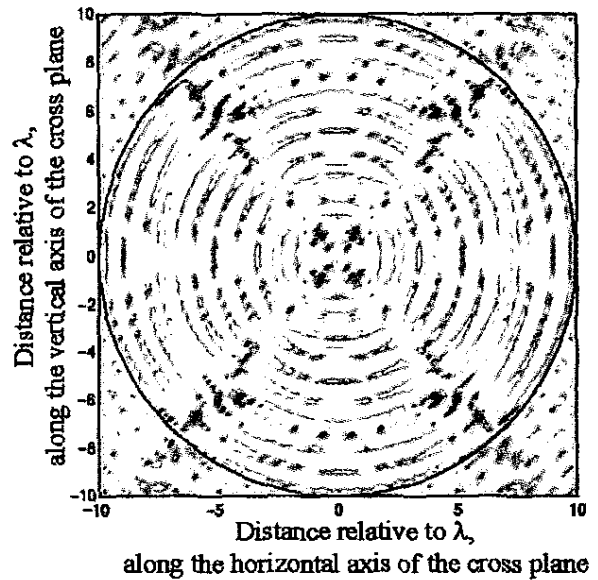


Figure 17c. The variations of the power-density criterion p_r/p_a for a 10λ radius aperture ($Rr/4 = 50\lambda$) on the transverse plane at 60λ from the aperture.

3.4 Aperture Shape Influence

Finally, we study the influence of the aperture's shape on the extent of the "very-near-field" region. Some square apertures with a uniform illumination have been studied. Figure 11 displays the variations of the E -field magnitude along the central axis of such apertures. The square apertures under study are 10λ , 20λ , and 50λ wide. Also, in these cases, the interference is less pronounced than in the case of the circular aperture. Indeed, the *Fresnel zones* – which present a rotational symmetry – are not matched for the square aperture. The outer *Fresnel zones* are not completely "filled up."

In order to determine the upper boundary of the "very-near-field" region of these apertures, we pinpointed the last minimum of the E -field magnitude. Once again, we arrived at a coefficient to apply to $Rr/4$. This time, the coefficient is higher than 1. For the three apertures of different dimensions, the coefficient is equal to 1.14.

4. Electromagnetic Characteristics of the "Very-Near-Field" Region of a Circular Uniform Aperture

If we now carefully compare the interference lobes of the E and the H fields for a 5λ -radius aperture with a uniform illumination (Figure 12), we can see that the E and H maximum magnitudes are not exactly similar. We can then assume that these two fields are not exactly in phase. Indeed, Figure 13 shows the phase shift between the E and H fields. This difference, first equal to $\pi/8$, tends to zero when the observation point moves away from the aperture. So, close to the aperture, the E and H fields are out of phase. Each peak of this last plot (Figure 13) corresponds to a minimum of the interference lobes of the field magnitude. The last one, located at one-quarter of the Rayleigh distance, points to a phase difference about 2° ; beyond, the fields can be considered to be in-phase.

The first consequence of this phase shift is that the wave impedance is complex, and therefore different from the free-space propagation impedance, which is $Z_0 = 120\pi$. The presence of some reactive power is the second consequence. Indeed, the power density is complex in this region, and it underlines the presence of a stationary wave, confined near the surface, in addition to a traveling wave that radiates. Both features are characteristic of the "very-near-field" region, and we now intend to study them.

4.1 Wave Impedance

Concerning the wave impedance, we use a criterion that is the relative difference between Z and Z_0 , that is, $|Z - Z_0|/Z_0$, (where $Z = E/H$ is the complex wave impedance and $Z_0 = 120\pi$). We point out that close to the aperture, Z is different from Z_0 , and we consider that outside the "very-near-field" region, the wave impedance has to be equal to Z_0 . This criterion has already been established in [1] to characterize the "very-near-field" region of a dipole antenna, and its limiting value has been adequately set there to be 0.01.

Figures 14a, 14b, and 14c show the variations of this criterion on the central perpendicular axis of the circular apertures stud-

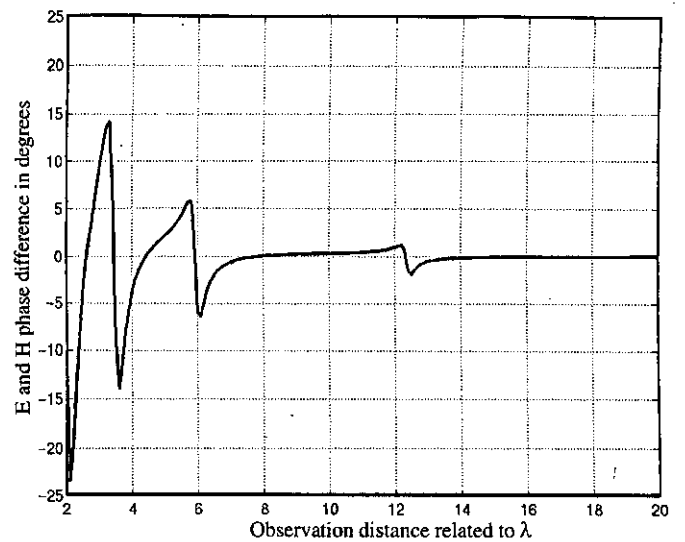


Figure 13. The phase shift between the E and H fields.

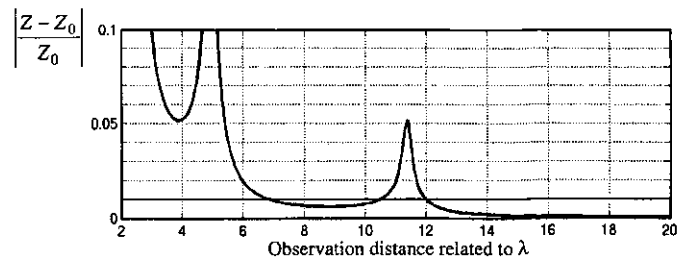


Figure 14a. The wave-impedance criterion for a 5λ radius circular aperture ($Rr/4 = 12.5\lambda$).

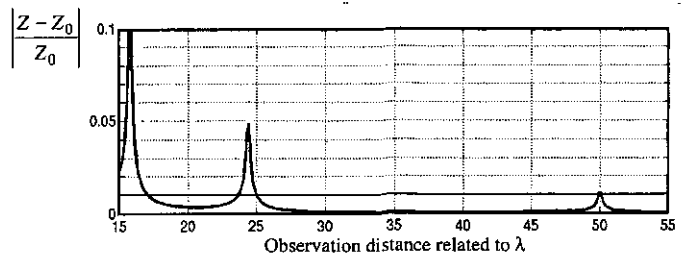


Figure 14b. The wave-impedance criterion for a 10λ radius circular aperture ($Rr/4 = 50\lambda$).

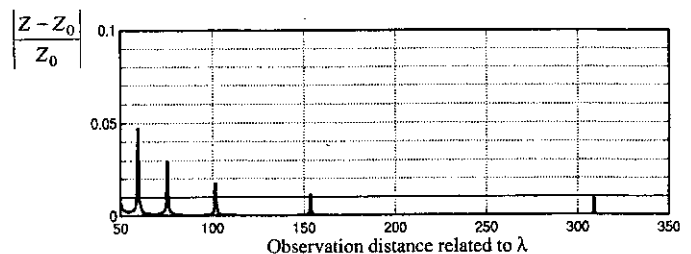


Figure 14c. The wave-impedance criterion for a 25λ radius circular aperture ($Rr/4 = 312.5\lambda$).

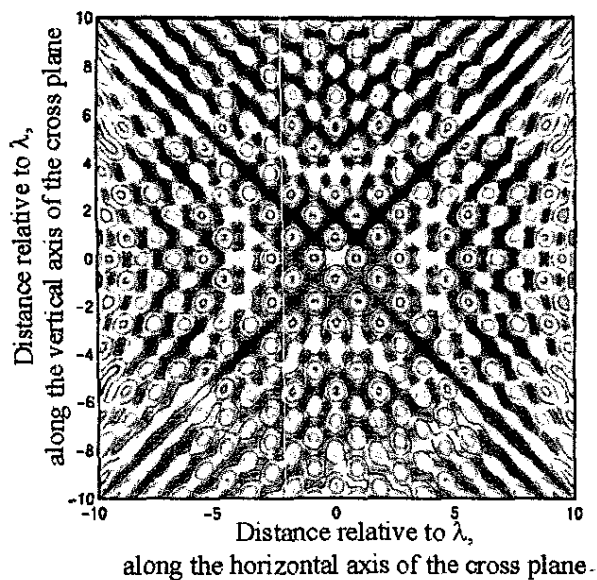


Figure 20a. The variations of the wave-impedance criterion $|Z - Z_0|/Z_0$ for a 20λ wide square aperture ($1.14Rr/4 = 57\lambda$) on the transverse plane at 15λ from the aperture.

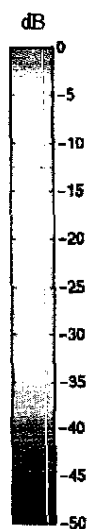


Figure 20b. The variations of the wave-impedance criterion $|Z - Z_0|/Z_0$ for a 20λ wide square aperture ($1.14Rr/4 = 57\lambda$) on the transverse plane at 30λ from the aperture.

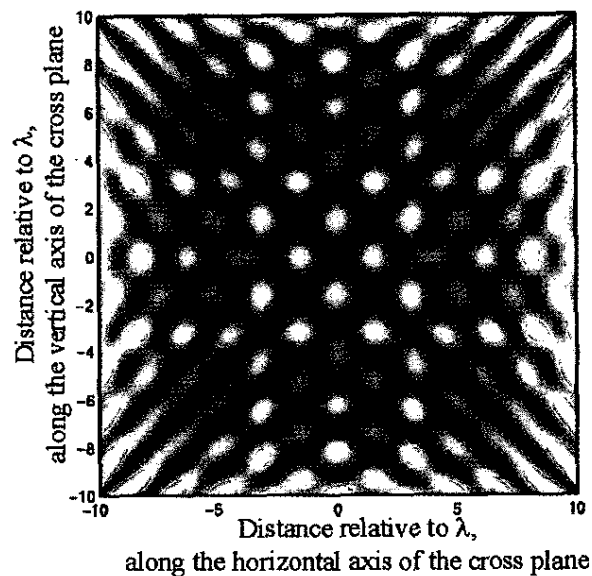


Figure 20b

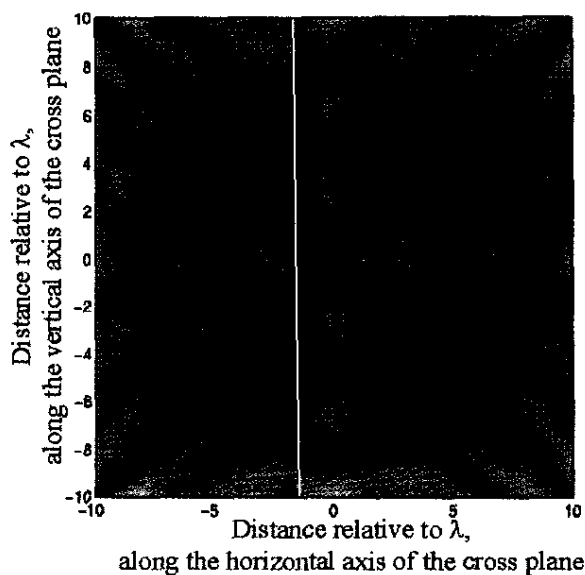


Figure 20c. The variations of the wave-impedance criterion $|Z - Z_0|/Z_0$ for a 20λ wide square aperture ($1.14Rr/4 = 57\lambda$) on the transverse plane at 60λ from the aperture.

Figure 20c

ied in the previous section. They also present definite peaks, corresponding once again to the minima of the field magnitude. We notice that the value of the criterion, 0.01, is reached exactly for one-quarter of the Rayleigh distance, i.e., just after the last peak, for the 5λ radius aperture, and just on the last peak for the 10λ and the 25λ radii apertures. Further than one-quarter of the Rayleigh distance, the criterion will be less than this limiting value, and we can consider that Z is equal to Z_0 .

4.2 Power Density

The criterion we use relative to the power density is the ratio of the imaginary and the real parts of the Poynting vector in the direction of propagation. This ratio, $\Im(p)/\Re(p) = p_r/p_a$, characterizes the presence of reactive power near the aperture. Again, this criterion was studied in [1] to investigate the “very-near-field” region of a dipole antenna, and a pertinent limit value was set at -30 dB (i.e., 10^{-3} in linear value). Indeed, for such a proportion we can consider that the reactive power is negligible, and so conclude that outside the “very-near-field” region there is no more reactive power.

Figures 15a, 15b, and 15c illustrate the variations of the power-density criterion on the central perpendicular axis of the same circular apertures as in Section 4.1. For the wave-impedance criterion, we can notice that the limiting value of the power-density criterion is reached for one-quarter of the Rayleigh distance, i.e., just after the last peak for the 5λ and 10λ radii apertures, or just on the last peak for the 25λ radius aperture.

The limiting values defined in [1] for the criteria concerning the wave impedance and the power density seem appropriate to the study of the circular uniform apertures. The results found in Sections 4.1 and 4.2 corroborate our conclusions of Section 3.1 about the upper boundary of the “very-near-field” region: this region extends from the aperture up to one-quarter of the Rayleigh distance.

4.3 Transverse Section Analysis in the “Very-Near-Field” Region

It is interesting to show the variations of these criteria, not only along the central perpendicular axis, but also on the transverse planes. Figures 16a, 16b, and 16c concern the wave-impedance criterion for the aperture of 10λ radius, and Figures 17a, 17b, and 17c illustrate the power-density criterion. For such an aperture, we saw that the upper boundary of the “very-near-field” region was located at 50λ . These graphics display the variations of both criteria on the transverse planes, located at distances of 15λ and 30λ from the aperture – thus, inside the “very-near-field” region – and at a distance of 60λ , outside this region. As we noted in the introduction, the radiation in the “near-field or Rayleigh” region is concentrated in a tubular beam. That is the reason why the transverse views are focused on this beam inside a circle of 10λ radius.

The transverse views in Figure 16 show that the impedance criterion, really disturbed inside the beam for a short observation distance, is higher than the limiting value of 0.01. According to these variations, we can conclude that inside the “very-near-field” region, Z isn’t equal to Z_0 . It tends to be uniform moving away

up to the “very-near-field” region boundary (50λ). At 60λ – so just after this limit – we can see that almost everywhere in the tubular beam the wave-impedance criterion is less than 0.01. There, Z is equal to Z_0 .

The power-density criterion presented in Figure 17 leads to the same conclusions as the impedance criterion. At 15λ , the ratio of the reactive power density is not negligible compared with the active power density, and up to 50λ we note some reactive power. So, all along the “very-near-field” region, there is still reactive power, first comparable to the active power, and then more and more negligible. At 60λ from the aperture and in the tubular beam of 10λ radius, there are as many points where the reactive-power criterion is greater than -30 dB as points where this criterion is less than -30 dB. But we can clearly see that the levels less than -30 dB often decrease down to -50 dB, whereas for only a few points do the levels greater than -30 dB reach -20 dB. So, we can say that the mean level is lower than -30 dB. Outside the “very-near-field” region, there is no more reactive power.

The conclusions from the study through the transverse planes and along the central perpendicular axis are coherent for this reference case. We can state that for a uniform circular aperture, the behavior of the criteria along the central axis is representative of what happens inside all of the tubular radiated beam. In view of

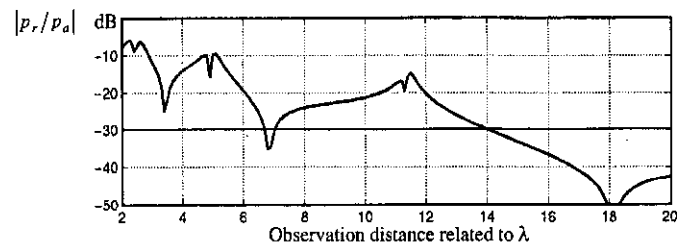


Figure 15a. The power-density criterion for a 5λ radius circular aperture ($Rr/4 = 12.5\lambda$).

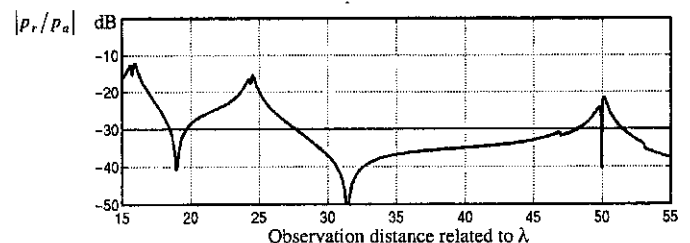


Figure 15b. The power-density criterion for a 10λ radius circular aperture ($Rr/4 = 50\lambda$).

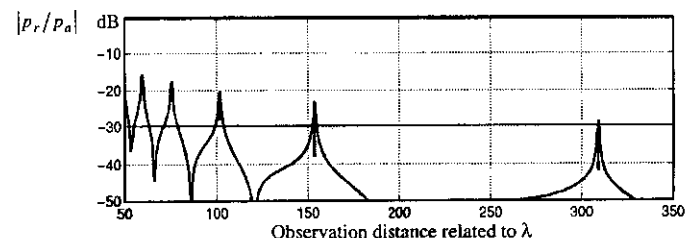


Figure 15c. The power-density criterion for a 25λ radius circular aperture ($Rr/4 = 312.5\lambda$).

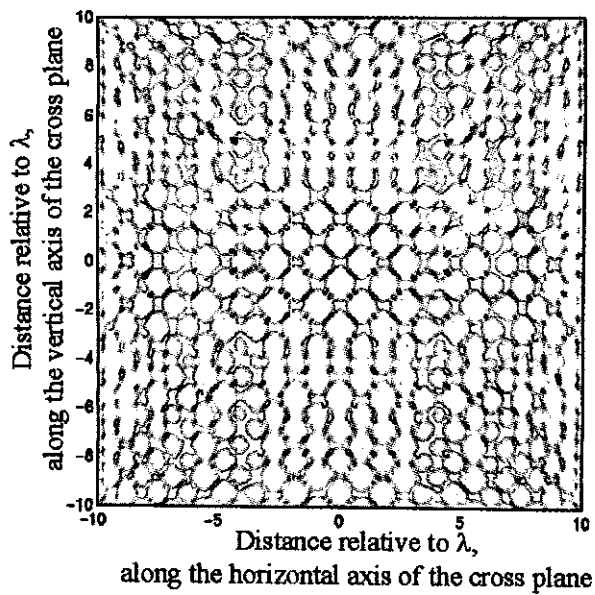


Figure 21a. The variations of the power-density criterion p_r/p_a for a 20λ wide square aperture ($Rr/4 = 57\lambda$) on the transverse plane at 15λ from the aperture.

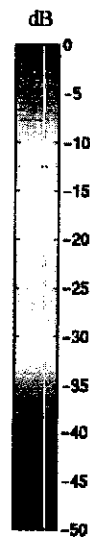


Figure 21b. The variations of the power-density criterion p_r/p_a for a 20λ wide square aperture ($Rr/4 = 57\lambda$) on the transverse plane at 30λ from the aperture.

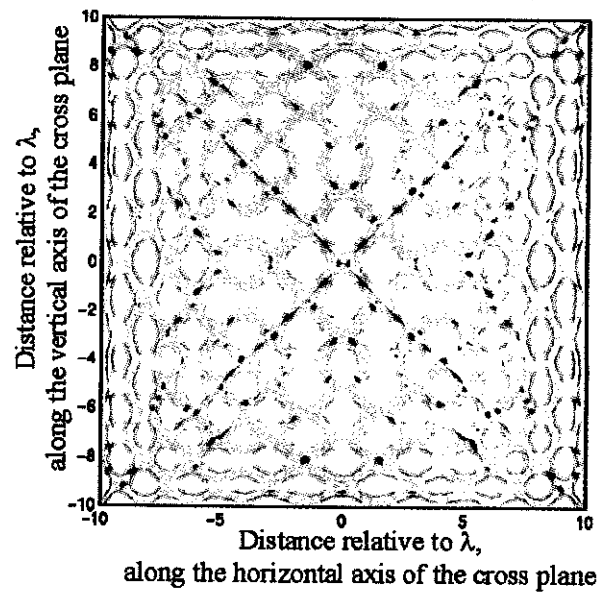
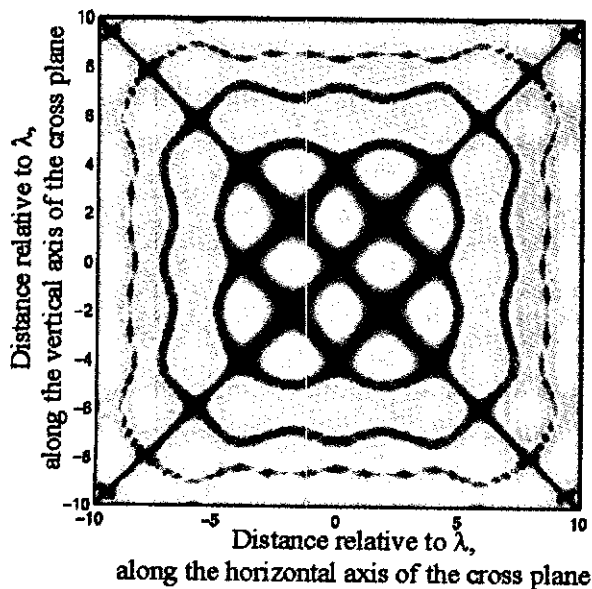


Figure 21c. The variations of the power-density criterion p_r/p_a for a 20λ wide square aperture ($Rr/4 = 57\lambda$) on the transverse plane at 60λ from the aperture.



these results, we can claim that the criteria for the wave impedance and the power density and their limiting values are adequate to define the boundary of the "very-near-field" region at $Rr/4$.

5. Electromagnetic Characteristics of the "Very-Near-Field" Region of a Square Uniform Aperture

In Section 2.4, we foresaw that the "very-near-field" region of a square aperture with a uniform illumination extended up to $1.14 Rr/4$, according to the interference location. We now study the two criteria mentioned above, first along the central axis and then through some transverse planes.

5.1 Wave Impedance

We explained in Section 2.4 that the interference along the central axis is less noteworthy in the square case than in the circular case. Consequently, the wave-impedance criterion variations for the square apertures do not present notable peaks. These varia-

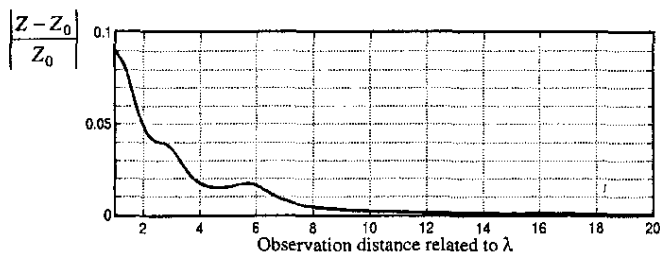


Figure 18a. The wave-impedance criterion for a 10λ wide square aperture ($1.14 Rr/4 = 14.5\lambda$).

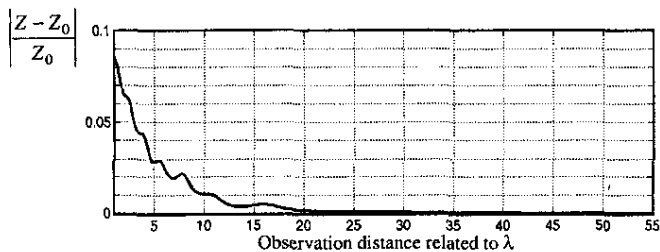


Figure 18b. The wave-impedance criterion for a 20λ wide square aperture ($1.14 Rr/4 \approx 57\lambda$).

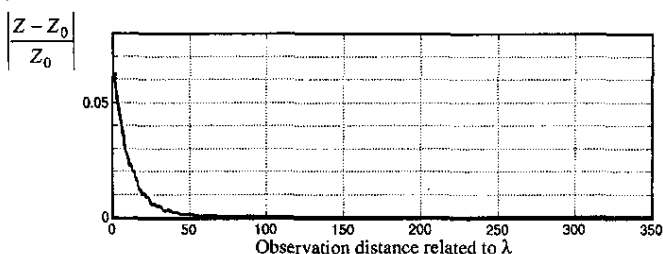


Figure 18c. The wave-impedance criterion for a 50λ wide square aperture ($1.14 Rr/4 \approx 356\lambda$).

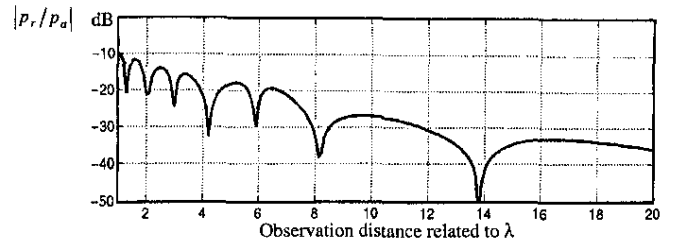


Figure 19a. The power-density criterion for a 10λ wide square aperture ($1.14 Rr/4 = 14.5\lambda$).

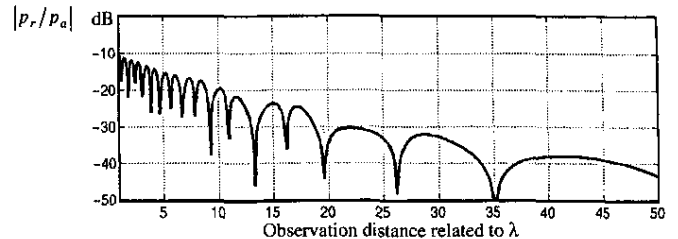


Figure 19b. The power-density criterion for a 20λ wide square aperture ($1.14 Rr/4 \approx 57\lambda$).

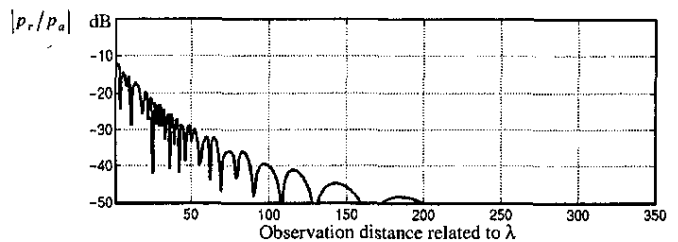


Figure 19c. The power-density criterion for a 50λ wide square aperture ($1.14 Rr/4 \approx 356\lambda$).

tions are shown in Figures 18a, 18b, and 18c for the 10λ to 50λ wide apertures. The limiting value of 0.01 is reached at distances really lower than $1.14 Rr/4$. The wave-impedance criterion along the central perpendicular axis does not seem really suitable for the square apertures, because it does not present a circular symmetry around this axis. The examination of this criterion on transverse planes would be rather more interesting.

5.2 Power Density

Figures 19a, 19b, and 19c present the variations of the power-density criterion for the same square apertures. In the same way, we can notice that the limiting value of -30 dB does not occur at distances about $1.14 Rr/4$, but closer to the aperture. Moreover, the distances deduced from this criterion are also different from the distances obtained from the impedance criterion. So, in the square-aperture case, we can assume that these two criteria are not consistent on the central axis. The study of these criteria on the transverse planes, presented in the next section, is all the more significant.

5.3 Transversal Section Analysis in the "Very-Near-Field" Region

This last part is important, because the radiation in the "near-field or Rayleigh" region is concentrated inside a square tubular beam. We will show that this study on the transverse planes will allow us to confirm the value of the "very-near-field" region boundary.

Figure 20 displays the variations of the wave-impedance criterion for a 20λ wide square aperture, for which the "very-near-field" region is extended up to 57λ . The first two figures (a and b) show this criterion on the transverse planes located at 15λ and 30λ , below this boundary. Referring to them, we can say that Z is not yet equal to Z_0 . At 60λ – that is, just after the "very-near-field" region boundary – the criterion is lower than the limiting value of 0.01. We can note from these views that the maximum values of the criterion are not located on the central axis, contrary to the circular case. This justifies the observation that the criterion on the central axis is not conclusive.

Figure 21 concerns the power-density criterion. It emphasizes that the "very-near-field" region boundary set at 57λ seems coherent. Indeed, the figures for the distances of 15λ and 30λ (Figures 21a and 21b) let us see that the reactive power density is not negligible compared with the active power density at such distances. For a distance of 60λ – just after the "very-near-field" region boundary – we can see that the power-density criterion is more or less than -30 dB inside the square tubular beam. As for the circular case, we do not have to consider the maximum value of the criterion inside the tubular beam, but rather its mean value. Indeed, the most important characteristic is the flux of the power density across the transverse section. So, at 60λ , the mean value of the power-density criterion is actually -30 dB.

Considering these last findings, we can assume that the boundary of $1.14Rr/4$ for the "very-near-field" region is well suited for the uniform square apertures. We can also conclude that the two criteria are consistent, even for the square-aperture case, providing that they are studied inside all of the tubular beam and not only along the central axis.

6. Conclusion

This paper has emphasized the specific characteristics of an equiphase aperture radiation in its "very-near-field" region, located at distances less than $D^2/8\lambda$ for the reference case of a uniform circular aperture. The upper boundary of this region is spread out between 0.69 and $0.82 D^2/8\lambda$ on a circular aperture for the main illumination laws tested, and it is set at $1.14 D^2/8\lambda$ for a uniform square aperture. The value $D^2/8\lambda$ represents one-quarter of the Rayleigh distance, $Rr = D^2/2\lambda$ (the "near-field" region boundary).

In concluding this work, it is worth pointing out a very simple and significant classification for the radiating regions of a circular equiphase aperture with a uniform illumination:

- The "very-near-field" region, from 0 to $Rr/4$, where the E and H fields are out of phase, the wave impedance is differ-

ent from 120π , and the power density is complex (reactive and active).

- The "near-field" region, between $Rr/4$ and Rr , where E and H are in phase, the wave impedance is equal to 120π , and the power density is active. This is the Rayleigh region for which the wave is quasi-planar inside a tubular beam.

- The "intermediate-field" (or Fresnel) region, between Rr and $4Rr$, where the wave is progressively transformed from a plane wave into a spherical wave, and the angular field distribution still depends on the distance from the antenna.

- The "far-field" (or Fraunhofer) region, beyond $4Rr$, inside which the radiation pattern of the antenna is formed, and where we have a quasi-spherical wave.

Finally, it is important to notice that the "very-near-field" region that has been characterized in this publication is more extended than the "near-field reactive" region located between 0 and $\lambda/2\pi$ by some authors [2]. Their definition is not pertinent, because at $\lambda/2\pi$, we still find as much reactive power density as active power density, and the wave impedance, Z , is not equal to 120π .

This work also has a practical interest for various applications in the wireless communications and radar antenna domains, as well as in electromagnetic compatibility, because the problem of direct or indirect radiation of antennas in their vicinity is growing.

7. References

1. S. Laybros and P. F. Combes, "On Radiating Zone Boundaries of Short, $\lambda/2$ and λ Dipoles," *IEEE Antennas and Propagation Magazine*, **45**, 5, October 2004, pp. 53-64.
2. "IEEE Standard Definitions of Terms for Antennas," *IEEE Transactions on Antennas and Propagation*, **AP-17**, 3, May 1969, pp. 252-259; and **AP-22**, 1, January 1974.
3. J. F. Ramsay, "Tubular Beams from Radiating Apertures," *Advances in Microwaves*, **III**, 1968, pp. 128-221.
4. P. F. Combes, "Etude de la Zone de Rayleigh des Ouvertures Circulaires par les Formules de Kottler et la Théorie Géométrique de la Diffraction," (Thèse de Doctorat sciences), *Revue du CETHEDC*, 78-2, 1978.
5. R. C. Hansen, *Microwave Scanning Antennas*, Los Altos, CA, Peninsula Publishing, 1985.
6. A. D. Yaghjian "An Overview of Near-Field Antenna Measurements," *IEEE Transactions on Antennas and Propagation*, **AP-34**, 1, January 1986, pp. 30-45.
7. C. A. Balanis, *Antenna Theory: Analysis and Design*, New York, John Wiley, 1982.
8. C. A. Balanis, *Advanced Engineering Electromagnetics*, New York, John Wiley, 1989, Chapter 6.
9. F. Kottler, "Electromagnetische Theorie der Beugung an Schwarzen Schirmen," *Annalen der Physik*, **71**, 1923, pp. 456.

10. J. A. Stratton and L. J. Chu, "Diffraction Theory of Electromagnetic Waves," *Physical Review*, **56**, 1939, pp. 99-107.
11. S. Silver, *Microwave Antennas Theory and Design*, New York, McGraw-Hill, 1949 (reprint: London, Peter Peregrinus Ltd., 1984).
12. S. Laybros, P. F. Combes, and H. J. Mametsa, "Very Near Field Zone Radiation of an Equiphase Circular Surface," *ICONIC*, Rouen, June 2003, pp. 28-31.

Introducing the Feature Article Authors

Sarah Laybros received the Diplôme d'Etudes Approfondies (postgraduate degree) in Microwave and Optical Telecommunications in 2001 from the Paul Sabatier University (UPS) of Toulouse (France). Since 2001, she has been a PhD student, both in the Microwave Antennas and Devices Laboratory of the Paul Sabatier University and in the Electromagnetic and Radar Department of the Office National d'Etudes et de Recherches Aérospatiales (ONERA). Her studies are dedicated to electromagnetic scattering from three-dimensional complex objects, taking into account their surrounding scene. A coupling of the Asymptotic Method formulations and the shooting and bouncing ray (SBR) technique has been developed in this aim. Her work on the computation of fields in complex scenes led her to investigate, on the one hand, the radiation zones of dipole and aperture antennas, and, on the other hand, the diffraction from metallic and impedance surfaces and wedges.

Paul-François Combes received the Doctorat de 3^{ième} Cycle and the Doctorat d'État es Sciences from the Toulouse

University, in 1968 and 1978, respectively. Since 1980, he has been a Professor of Microwave and Head of the Microwave Antennas and Devices Laboratory of the Paul Sabatier University of Toulouse. He is also in charge of the doctoral training in "Microwave and Optical Telecommunications." He has been the supervisor of 30 doctoral theses of the Paul Sabatier University of Toulouse, and is currently conducting two theses. He is author and/or co-author of about 100 publications covering the fields of reflector and array antennas, propagation of electromagnetic waves, radar, and radiometric and polarimetric devices for millimeter waves. In addition, he is the author of eight books, including *Microwave Transmission for the Telecommunications* (Wiley, 1991; second edition, 1995) and *Micro-ondes: Lignes, Guides et Cavités, Volume 1* and *Micro-ondes: Circuits Passifs, Propagation, Antennes, Volume 2* (Dunod, 1996, 1997, in French).

Henri-José Mametsa received the Diploma in Telecommunication Engineering and the PhD degree in Electronics from the Ecole Nationale des Télécommunications de Bretagne (France) in 1984 and 1986, respectively. For two years he worked as an engineer in the Antenna Design Department of Thomson-CGR. In 1987, he joined the Electromagnetic and Radar Department of the Office National d'Etudes et de Recherches Aérospatiales (ONERA), where he has been working on different studies in electromagnetic scattering problems. In 1995, he spent a year on sabbatical at the Defence Research Establishment in Ottawa (Canada), where he worked on remote-sensing polarimetry. His current research interests include modeling electromagnetic scattering from man-made targets and natural media. Principal applications were developed in the asymptotic electromagnetic formulations coupling with the shooting and bouncing rays technique. He co-directed six PhD students during the last two years. (✉)

IEEE Antennas and Propagation Magazine, Vol. 47, No. 4, August 2005